Nucleic Acids Research Advance Access published February 7, 2012

Nucleic Acids Research, 2012, 1–15
doi:10.1093/nar/gks025

Dataset integration identifies transcriptional regulation of microRNA genes by PPARγ in differentiating mouse 3T3-L1 adipocytes

Elisabeth John[1], Anke Wienecke-Baldacchino[1], Maria Liivrand[1], Merja Heinäniemi[1], Carsten Carlberg[1,2] and Lasse Sinkkonen[1,*]

[1]Life Sciences Research Unit, University of Luxembourg, L-1511 Luxembourg, Luxembourg and [2]Department of Biosciences, University of Eastern Finland, FIN-70211 Kuopio, Finland

Received September 7, 2011; Revised December 23, 2011; Accepted January 4, 2012

ABSTRACT

Peroxisome proliferator-activated receptor γ (PPARγ) is a key transcription factor in mammalian adipogenesis. Genome-wide approaches have identified thousands of PPARγ binding sites in mouse adipocytes and PPARγ upregulates hundreds of protein-coding genes during adipogenesis. However, no microRNA (miRNA) genes have been identified as primary PPARγ-targets. By integration of four separate datasets of genome-wide PPARγ binding sites in 3T3-L1 adipocytes we identified 98 miRNA clusters with PPARγ binding within 50 kb from miRNA transcription start sites. Nineteen mature miRNAs were upregulated ≥2-fold during adipogenesis and for six of these miRNA loci the PPARγ binding sites were confirmed by at least three datasets. The upregulation of five miRNA genes miR-103-1 (host gene *Pank3*), miR-148b (*Copz1*), miR-182/96/183, miR-205 and miR-378 (*Ppargc1b*) followed that of *Pparg*. The PPARγ-dependence of four of these miRNA loci was demonstrated by PPARγ knock-down and the loci of miR-103-1 (*Pank3*), miR-205 and miR-378 (*Ppargc1b*) were also responsive to the PPARγ ligand rosiglitazone. Finally, chromatin immunoprecipitation analysis validated *in silico* predicted PPARγ binding sites at all three loci and H3K27 acetylation was analyzed to confirm the activity of these enhancers. In conclusion, we identified 22 putative PPARγ target miRNA genes, showed the PPARγ dependence of four of these genes and demonstrated three as direct PPARγ target genes in mouse adipogenesis.

INTRODUCTION

The need for understanding of the mechanisms controlling the differentiation of fibroblast-like pre-adipocytes to lipid-loaded adipocytes is due to the worldwide epidemic of obesity of high medical relevance (1). Adipogenesis is regulated by a network of transcription factors. The most prominent transcription factor in adipocytes is the nuclear receptor peroxisome proliferator-activated receptor γ (PPARγ) (2). During mouse adipogenesis the number of genomic binding sites for PPARγ increases from a few to thousands (3–7) implicating that PPARγ regulates hundreds of genes during adipogenesis. Therefore, the synthetic PPARγ ligand rosiglitazone (RGZ) has been used in many countries in the therapy of type 2 diabetes mainly acting via its effects on gene regulation in adipocytes (8).

The prerequisite for the direct transcriptional regulation of a given gene by PPARγ is the presence of at least one specific PPARγ binding site, referred to as PPAR response element (PPRE), in the regulatory regions flanking the gene's transcription start site (TSS) [reviewed in (9)]. Direct DNA binding of PPARγ takes place as a heterodimeric complex with another nuclear receptor, the retinoid X receptor (RXR), and PPREs are formed as a direct repeat of hexameric core binding motifs with one intervening nucleotide (DR1-type PPREs) (10,11). To promote the expression of its target genes, PPARγ must overcome the transcriptionally repressive dense packaging of genomic DNA within chromatin. PPARγ is also capable of repressing some of its target genes in a ligand-dependent manner either directly via recruitment of co-repressors upon agonist binding or via a mechanism called trans-repression (12,13). However, in adipocytes PPARγ has been mainly linked to transcriptional activation of its target genes (3–5).

*To whom correspondence should be addressed. Tel.: +352-4666446839; Fax: +352-4666446949; Email: lasse.sinkkonen@uni.lu

In addition to transcription factors and their co-factors, several new groups of small RNA molecules have been described in recent years as capable of controlling gene expression [reviewed in (14)]. One of the most important of these groups consists of small RNA molecules called microRNAs (miRNAs), which are endogenous non-coding transcripts transcribed mainly by RNA polymerase II (RNA Pol II) as their own primary transcripts (pri-miRNAs) or together with their host genes [reviewed in (15)]. The miRNA precursor (pre-miRNA) is cropped from the primary transcript by a complex known as Microprocessor that consists of two proteins, namely DROSHA and DGCR8. This pre-miRNA hairpin is then further processed into the mature miRNA duplex by an RNase III enzyme DICER. The mature miRNAs can identify their target mRNAs by base pairing to the partially complementary regions within the target mRNAs (16). miRNAs function by serving as guides to the proteins of the Argonaute family and other associated proteins, which together induce inhibition of translation as well as degradation of the targeted mRNAs (17,18). Currently, there are more than 700 known mature miRNAs in mouse (miRBase v18.0) and most of them can potentially target hundreds of mRNAs (19,20). In this way they show very comparable functions to transcription factors. Thus miRNAs can remarkably influence the transcriptomes of most eukaryotic cells. Still, fairly little is known about the transcriptional regulation of miRNA genes. Until recently, the progress was hampered by limited knowledge about the structure of miRNA genes, especially the location of their TSSs (21,22). Many miRNAs are transcribed together as clusters of several mature miRNAs. Considering this feature and the fact that each of these miRNAs can have a potential to regulate a vast number of target mRNAs, the transcriptional control of these miRNA genes needs to be both accurate and robust. And importantly, miRNAs have been shown to play key roles in the development and differentiation of most tissues and cell types (23). Also the formation of white adipose tissue *in vivo* and the differentiation of the mouse pre-adipocyte cell line 3T3-L1 depend on expression of miRNAs (24,25). Moreover, some miRNAs, such as miR-103, are regulators of adipogenesis in mouse (26).

Several recent datasets of chromatin immunoprecipitation (ChIP)-based monitoring of genome-wide binding of PPARγ during differentiation of 3T3-L1 cells identified thousands of genomic PPARγ-bound sites suggesting hundreds of PPARγ target genes (3–7). However, none of these are miRNA genes. Therefore, in this study we integrated four of the above mentioned datasets of genome-wide PPARγ binding sites and mouse miRNA TSS annotations (3–6,21) and identified 98 miRNA clusters with PPARγ binding within 50 kb from miRNA gene TSSs. Nineteen of these miRNAs (corresponding to 22 miRNA genes) are upregulated during adipogenesis and are putative PPARγ targets. Further filtering resulted in the five miRNA genes miR-103-1 (host gene *Pank3*), miR-148b (*Copz1*), miR-182/96/183, miR-205 and miR-378 (*Ppargc1b*) that followed the upregulation of the *Pparg* gene during mouse adipogenesis. The transcription of all except miR-148b (*Copz1*) depends on PPARγ in adipocytes and the loci of miR-103-1, miR-205 and miR-378 were also responsive to RGZ. Finally, ChIP assays validated three *in silico* predicted PPREs at the miR-103-1 locus, two at the miR-378 locus, and one at the miR-205 locus. In conclusion, we have identified a number of PPARγ-regulated miRNA genes in mouse adipogenesis, which will serve the future integration of miRNAs to the core regulatory network of adipocyte differentiation and further characterize the extensive role of PPARγ during this process.

MATERIALS AND METHODS

Integration of the genome-wide PPARγ binding data and miRNA TSS annotation

The different publically available datasets used in this study were unified on a common genome build on the basis of the coordinates from TSS annotation data for miRNA genes from Marson *et al.* (21), namely NCBI36/mm8. Accordingly, the coordinates of the PPARγ-bound sites from Nielsen *et al.* (4) and Lefterova *et al.* (6) were lifted over from mm9 to mm8 using the UCSC lift-over tool, while the coordinates from the datasets of Lefterova *et al.* (3) and Hamza *et al.* (5) were already based on mm8. For all datasets we used only published pre-analyzed data and the provided coordinates for PPARγ-bound sites were used. First, miRNA gene TSSs within 50 kb of a PPARγ binding site (Supplementary Table S1A–D) were identified. This was followed by checking whether an identified PPARγ binding site overlaps with an *in silico* predicted PPRE (10) (Supplementary Table S2A–D). A third step detects, whether an identified PPARγ binding site co-localizes with a CEBPα (CCAAT/enhancer binding protein) binding site. As input data for the last step, PPARγ- and CEBPα-bound sites provided by Lefterova *et al.* (3) were used and a threshold of 1 kb was applied to define a co-localized region. Further details can be provided upon request.

Cell culture

The 3T3-L1 mouse pre-adipocyte cell line was used for all experiments. The cells were maintained in Dulbecco's modified Eagle's medium supplemented with 10% fetal calf serum, 1% penicillin–streptomycin and 1% L-glutamine. The cells were kept at 37°C and 5% CO_2. In order to differentiate pre-adipocytes to adipocytes, the cells were seeded 4 days before differentiation (D-4), grown 2 days to reach confluency (D-2) and maintained 2 days post-confluency before starting the differentiation (D0) by adding differentiation medium I (500 µM 3-isobutyl-1-methylxanthine, 250 nM dexamethasone and 5 µg/ml insulin in normal growth medium). From D2 on differentiation medium II (5 µg/ml insulin and 100 nM RGZ in normal growth medium) was used and renewed every 2 days (D4, D6). For treatments with RGZ and 5,6-Dichlorobenzimidazole 1-β-D-ribofuranoside (DRB) the cells were seeded and grown in the same way as described above. Two or six days differentiated 3T3-L1 mouse cells were treated either with 100 nM RGZ

or 100 μM of DRB and with an equal volume of a vehicle control [dimethyl sulfoxide (DMSO)] and total RNA was collected after 4, 8, 12, 24 and 48 h.

siRNA silencing

Six days differentiated 3T3-L1 cells were transfected with Nucleofector II Device (Lonza, Basel, Switzerland) by using Cell Line Nucleofector Kit V and program A-033. The transfection procedure was done according to the manufacturer's instructions using a 100 nM mixture of three double-stranded siRNA sequences against *Pparg* (si*Pparg*, Eurogentec, Liege, Belgium) or 100 nM of a scrambled double-stranded siRNA sequence as a control (si*Control*, Eurogentec). The cells were collected 48 h post-transfection. The siRNA sequences are provided in Supplementary Table S3.

RNA extraction and cDNA synthesis

Total RNA was isolated from the 3T3-L1 cells by using TRIsure (Bioline, London, UK). Medium was removed and 1 ml of TRIsure per 6-well plates was added to lyse the cells. RNA was extracted with 200 μl chloroform and precipitated from the aqueous phase with 400 μl isopropanol by incubating at −20°C overnight. cDNA was synthesized by using 1 μg of total RNA, 0.5 mM dNTPs, 2.5 μM oligo-dT primer (for mature mRNAs) or 0.2 μg random hexamer primers (for pri-miRNAs), 1 U/μl RiboLock RNase Inhibitor (Fermentas, Vilnius, Lithuania) and 10 U/μl M-MuLV Reverse Transcriptase (Fermentas). The cDNA synthesis was performed for 1 h at 37°C and the reaction was stopped by 10 min incubation at 70°C.

Quantitative PCR

Real-time quantitative PCR (qPCR) was performed in an Applied Biosystems 7500 Fast Real-Time PCR System using Absolute Blue qPCR SYBR Green Low ROX Mix (Thermo Fisher Scientific, Surrey, UK). For each reaction 5 μl of cDNA template or 4 μl of ChIP template, 1 μl of primer pairs (10 μM) and 10 μl of the qPCR SYBR mixture to a final reaction volume of 20 μl were used. The PCR reaction started with 15 min at 95°C to activate the polymerase. The PCR cycling conditions were: 40 cycles, of which each was composed of 15 s at 95°C, 15 s at 55°C and 30 s at 72°C. Relative expression levels at the tested experimental conditions were calculated within each independent experiment using the formula $2^{-(\Delta\Delta Ct)}$, where $\Delta\Delta Ct$ is $(Ct_{(\text{target gene})} - Ct_{(Rpl13a)})_{\text{tested condition}} - (Ct_{(\text{target gene})} - Ct_{(Rpl13a)})_{\text{control condition}}$ and the Ct is the cycle, at which the threshold is crossed. Depending on the experiment either vehicle control, si*Ctrl* or D0 served as the control condition. The quality of the PCR product was monitored using post-PCR melt curve analysis. The sequences of the primer pairs are listed in Supplementary Table S4 and a schematic depiction of their locations is provided in Supplementary Figure S1.

miRNA assays

The detection of the miRNAs was done by using TaqMan MicroRNA Reverse Transcription Kit together with TaqMan MicroRNA Assays (Applied Biosystems). The miRNA cDNA synthesis and miRNA detection was done by following the manufacturers instructions and by using an Applied Biosystems 7500 Fast Real-Time PCR System. Relative expression levels at the tested experimental conditions were calculated within each independent experiment using the formula $2^{-(\Delta\Delta Ct)}$, where $\Delta\Delta Ct$ is $(Ct_{(\text{target miRNA})} - Ct_{(U6)})_{\text{tested condition}} - (Ct_{(\text{target miRNA})} - Ct_{(U6)})_{\text{control condition}}$ and the Ct is the cycle, at which the threshold is crossed. Depending on the experiment either vehicle control, si*Ctrl* or D0 served as the control condition.

ChIP

ChIP was performed using confluent 3T3-L1 pre-adipocytes (D0) or 3T3-L1 adipocytes (D6) grown on 10 cm^2 dishes. Chromatin was cross-linked by adding formaldehyde at final concentration of 1% to the culture media for 8 min. The cross-linking reaction was stopped with 150 mM glycine for 5 min. The cells were washed twice with phosphate-buffered saline (PBS) and lysed in 650 μl SDS lysis buffer (1% SDS, 10 mM EDTA, 50 mM Tris–HCl, pH 8.1) containing a protease inhibitor cocktail (Roche Diagnostics, Mannheim, Germany). In order to reduce the DNA to average length of 500 bp, the lysates were sonicated (Bioruptor, Diagenode, Liege, Belgium) with 15 × 30 s pulses. Cellular debris were removed by centrifugation and the lysates were diluted 1:10 in ChIP dilution buffer (0.01% SDS, 1.1% Triton X-100, 1.2 mM EDTA, 167 mM NaCl, protease inhibitors and 16.7 mM Tris–HCl, pH 8.1). A quantity of 1500 μl of diluted lysate were incubated with the respective antibody [3.5 μl anti-PPARγ (101 700, Cayman, Ann Arbor, MI USA), 5 μl anti-PPARγ (sc-7196, Santa Cruz Biotechnologies, Santa Cruz, CA, USA) or 2.5 μl IgG (sc-2027)] overnight at 4°C. The immuno-complexes were collected with 60 μl of BSA-coated protein A agarose beads slurry (Millipore, Billerica, MA, USA) for 2 h at 4°C with rotation. The beads, containing the immuno-complexes, were washed sequentially with 1 ml of the following buffers: low salt wash buffer (0.1% SDS, 1% Triton X-100, 2 mM EDTA, 150 mM NaCl, 20 mM Tris–HCl, pH 8.1), high salt wash buffer (0.1% SDS, 1% Triton X-100, 2 mM EDTA, 500 mM NaCl, 20 mM Tris–HCl, pH 8.1), LiCl wash buffer (0.25 mM LiCl, 1% Nonidet P-40, 1% sodium deoxycholate, 1 mM EDTA, 10 mM Tris–HCl, pH 8.1) and twice with TE buffer (1 mM EDTA, 10 mM Tris–HCl, pH 8.0). After the washing steps the immuno-complexes were eluted with 500 μl elution buffer (1% SDS, 100 mM $NaHCO_3$). The cross-linking was reversed with proteinase K (40 μg/ml, Fermentas) overnight at 65°C. The DNA was recovered by phenol-chloroform extraction or by ChIP DNA Clean Kit (Zymo Research, Irvine, CA, USA), ethanol precipitated and dissolved in 60 μl of water. Sample of 4 μl were used as template for qPCR using specific primers listed in Supplementary Table S4. Relative enrichment was calculated using the formula $2^{-(\Delta\Delta Ct)}$ where $\Delta\Delta C_t$ is $(Ct_{(PPAR\gamma)} - Ct_{(\text{input})}) - (Ct_{(IgG)} - Ct_{(\text{input})})$, PPARγ and IgG are the respective immunoprecipitated

DNA samples and input is 1:100 diluted purified genomic DNA from the starting material of the respective immunoprecipitation.

Western blot

Cells, seeded in 6-well plates, were first washed with PBS, trypsinized for 5 min at 37°C and centrifuged. The remaining pellet was lysed in 200 µl ice-cold protein lysis buffer (150 mM NaCl, 1 mM EDTA, 1% Triton-X, 20 mM Tris–HCl, pH 7.4) containing protease inhibitors (Roche Diagnostics). Then the lysate was sonicated at low frequency with 10 repeats of 8 s pulses followed by 30 s pauses. Sonicated lysates were centrifuged for 30 min at maximum speed to separate the fat from the proteins and the cell debris. The protein concentrations were measured by Bradford assay and comparable amounts were loaded on a gel. The proteins were separated with SDS–PAGE, probed with the corresponding primary (anti-PPARγ, 1:200 dilution (101 700 Cayman), anti-β-actin, 1:10,000 dilution (MAB1501, Millipore) and horseradish peroxidase-coupled secondary antibodies (anti-mouse IgG, 1:500 dilution (P0447, Dako, Glostrup, Denmark) and anti-rabbit IgG, 1:500 dilution (P0448, Dako)) and detected via ECL (GE Healthcare, Buckinghamshire, UK).

RESULTS

PPARγ localization at miRNA loci in mouse adipocytes

In order to identify miRNA genes regulated by PPARγ in mouse adipogenesis, we integrated the genome-wide binding site coordinate information from four available datasets (3–6) with the recent TSS annotation of mouse miRNA genes (21) (Table 1). The considered binding sites were selected according to the analysis in the original publications (3–6). The total number of PPARγ-bound sites in the differentiated 3T3-L1 adipocytes varied for each dataset from approximately 2600 to almost 7000. We screened each of the four datasets for miRNA genes that had at least one PPARγ-bound site within ±50 kb from their TSS (Supplementary Table S1). Under these criteria for each dataset between 22 and 70 miRNA clusters (corresponding to 31–113 miRNA precursors) were identified. Combining the information from all four datasets resulted in 98 different miRNA clusters (corresponding to 149 individual miRNA precursors and 140 different mature miRNAs, Table 1). Within these 98 genomic loci 61 miRNA genes had at least one of their observed PPARγ-bound sites overlapping with a putative PPRE identified *in silico* by RESearch algorithm (10) (summarized in Table 1, details are in Supplementary Table S2). This suggests that in majority of the loci the PPARγ enrichment corresponds to direct DNA binding.

In summary, we integrated genome-wide datasets for PPARγ binding with the location of miRNA gene TSSs and identified 149 pre-miRNAs corresponding to 140 mature miRNAs in 98 genomic loci with at least one PPARγ binding site within 50 kb distance to their TSS.

Identification of putative PPARγ target miRNA genes

To better distinguish, which of the miRNA genes with PPARγ binding in their vicinity could be direct targets of PPARγ, we compared the list of 140 mature miRNAs combined from all four datasets (originating from 149 precursors; Table 1) to the existing miRNA expression profiling from 3T3-L1 adipocytes (26) (Figure 1A). Applying a 2-fold cut-off, a similar number of miRNAs were up- and downregulated (26 and 19, respectively) during 9 days of adipogenesis. Comparing these miRNA lists with the combined list of 140 mature miRNAs (Table 1) showed that a total of 19 different mature miRNAs associated with PPARγ binding in at least one of the datasets were also upregulated above 2-fold during 3T3-L1 adipogenesis (Figure 1A). Nine different miRNAs showed similar extent of downregulation. Interestingly, the miRNA genes with PPARγ-bound sites were significantly enriched for upregulated miRNAs (calculated using hypergeometric probability, $P = 1.03 \times 10^{-5}$). This enrichment of upregulated miRNAs fits well with the role of PPARγ as a transcriptional activator of its target genes (3–5) and implies that many of these miRNAs could be real targets of PPARγ-mediated regulation.

Since many mature miRNAs can be transcribed from more than one locus, but cannot be distinguished by sequence in miRNA microarray analysis, the number of miRNA genes that are putative primary PPARγ targets is 22, i.e. it exceeds that of the identified mature miRNAs. In addition, many of these putative PPARγ target miRNA genes give rise to more than one mature miRNA. This opens the possibility that also the other miRNAs that are transcribed from these clusters are regulated by PPARγ, although they did not change above 2-fold in the array analysis.

Table 1. Genome-wide PPARγ occupancy close to miRNA gene TSSs

Dataset	Total # of PPARγ peaks	# of miRNA precursors with PPARγ peak (±50 kb)	# of miRNA clusters with PPARγ peak (±50 kb)	# of miRNA clusters with PPARγ peaks overlapping PPREs
Lefterova *et al.* (3) (ChIP-chip)	5299	77	52	36
Nielsen *et al.* (4) (ChIP-Seq)	6946	113	70	45
Hamza *et al.* (5) (ChIP-PET)	2953	49	35	1
Lefterova *et al.* (6) (ChIP-Seq)	2611	31	22	12
All combined	–	149	98	61

The annotation of miRNA TSS is based on Marson *et al.* (21).

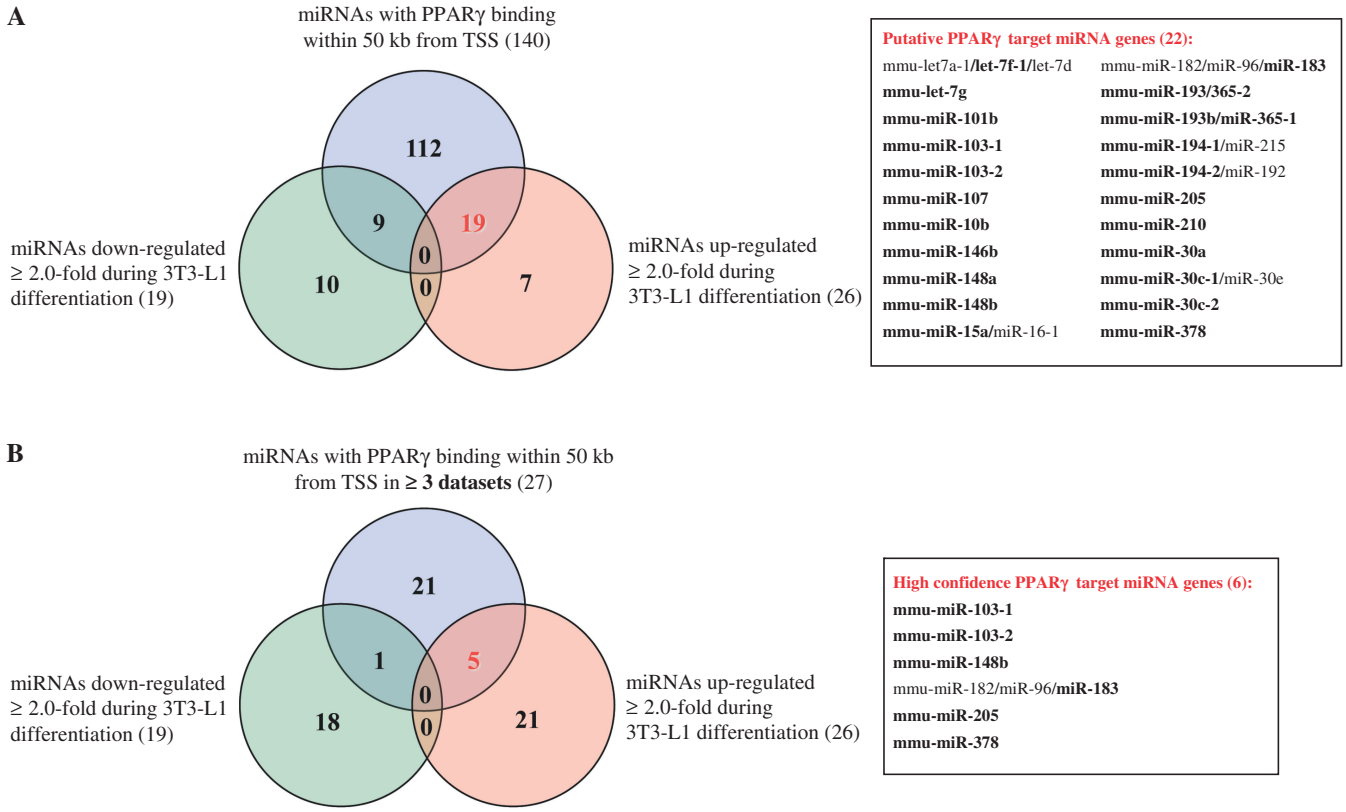

Figure 1. Dataset integration to identify the putative PPARγ target miRNAs. (**A**) A Venn diagram depicting the overlapping of the list of all individual mature miRNAs (140) with PPARγ binding within 50 kb from their TSS (Supplementary Table S1) together with >2-fold up or downregulated miRNAs based on available miRNA expression profiling during 3T3-L1 differentiation (26). This analysis yields 19 upregulated mature miRNAs that are putative PPARγ targets. The 22 putative PPARγ target miRNA genes corresponding to the 19 mature miRNAs (in bold) are listed on the right side. (**B**) A Venn diagram depicting the overlapping of the list of all individual mature miRNAs (27) with PPARγ binding within 50 kb from their TSS (Supplementary Figure S2) in at least three of the used datasets together with >2-fold up or downregulated miRNAs based on available miRNA expression profiling during 3T3-L1 differentiation. This analysis yields five upregulated mature miRNAs that are high confidence PPARγ targets. The six putative PPARγ target miRNA genes corresponding to the five mature miRNAs (in bold) are listed on the right side.

In order to more stringently identify the true targets of PPARγ among the putative target miRNAs, we analyzed how many of all of the miRNA genes are implicated as PPARγ targets in at least three of the four used genome-wide binding profile datasets. The direct overlapping of the exact PPARγ binding site genomic coordinates from the four different datasets rarely show direct matches, although the same antibody has been used in all four studies (data not shown). These differences are likely to be explained by the rather different methodology and varying data analysis strategies. In order to overcome this issue, we checked how many of the PPARγ-associated miRNAs (Supplementary Table S1) were common between the different datasets. Ten miRNAs were located in loci bound by PPARγ in all four genomic PPARγ binding site datasets and another 19 in at least three of the four datasets (Supplementary Figure S2). From these 29 miRNAs, 27 were mature miRNAs with different sequences and could be distinguished in miRNA microarray analysis. Overlapping the list of these mature miRNAs with the miRNAs downregulated in adipocytes yielded only one mature miRNA (Figure 1B). However, five mature miRNAs miR-103, miR-148b, miR-183, miR-205 and miR-378, originating from six separate miRNAs genes, were upregulated above 2-fold in adipocytes. These constitute the high confidence PPARγ target miRNA genes in mouse adipocytes and are referred to as the candidate PPARγ target miRNAs from here on.

Taken together, further filtering of miRNA genes with PPARγ-bound sites that were both confirmed in at least three genome-wide datasets and upregulated at least 2-fold during adipogenesis reduced the list to the five miRNAs miR-103, miR-148b, miR-183, miR-205 and miR-378.

Dynamic expression profiles of the candidate PPARγ-target miRNAs and their host genes during adipocyte differentiation

The five candidate PPARγ target miRNAs originate from six different miRNA loci, since miR-103 is transcribed from two different loci, miR-103-1 and miR-103-2, as two identical mature miRNAs. miR-103-1, miR-103-2, miR-148b and miR-378 are transcribed within their respective host genes *Pank3*, *Pank2*, *Copz1* and *Ppargc1b*. None of these host genes have so far been described as

primary PPARγ targets. miR-183 and miR-205 are transcribed from intergenic regions, most likely as independent miRNA genes. In addition, miR-183 is part of a cluster of three mature miRNAs and is transcribed together with the two other members of the cluster, miR-182 and miR-96.

Due to the very short sequence of the mature miRNAs, the arrays used to measure miRNA expression profiles are often prone to false positive results. In order to validate the upregulation and to analyze the expression dynamics of the six candidate PPARγ target miRNAs as well as their host genes, we profiled their expression and compared them with the positive control genes *Pparg*, *Cebpa* and *Angptl4* during mouse adipogenesis. To do this we took every 24 h RNA samples from the 8-day differentiation process of 3T3-L1 cells and determined by qPCR the relative expression of the transcripts of interest (Figure 2A). For each miRNA we measured the levels of the mature miRNA as well as the pri-miRNA. While the exact fold changes between independent differentiation experiments vary, the overall expression profiles of individual transcripts were generally reproducible (Figure 2B–G). This was confirmed by ANOVA analysis for significant changes during the time course, which confirmed the changes for all tested mRNAs and most of the microRNAs as statistically significant (Figure 2).

The robust upregulation of the *Pparg* gene was visible already on D2 and confirmed the successful differentiation of the adipocytes (Figure 2B). The expression profiles of the two known primary PPARγ target genes, *Cebpa* and *Angptl4* (27,28), followed closely that of *Pparg*. All three genes were clearly induced by D4 and remained at induced levels through the remaining time course (Figure 2B).

Mature miR-103-1 and miR-103-2 are produced from intron 5 of two separate but related host genes encoding the pantothenate kinases PANK3 and PANK2, respectively. These enzymes are important for co-enzyme A synthesis and thereby for lipid metabolism (29). The level of mature miR-103 continuously increased through the differentiation starting from D2 to >5-fold on D8 (Figure 2C). Consistent with previous reports, the *Pank2* gene showed no or only weak upregulation during adipogenesis when compared with the level of *Pank3* mRNA that robustly increased with an expression profile similar to that of the known PPARγ target gene *Cebpa* (Figure 2C) (26). This indicates that the observed increase in miR-103 is mainly due to increased production of miR-103-1 from the *Pank3* gene locus. This observation is further supported by the fact that pri-miR-103-1 is clearly induced during adipogenesis while pri-miR-103-2 remained non-induced in most experiments. Interestingly, the upregulation of the mature miR-103 showed a delay in relation to its host gene *Pank3*. This might reflect the different processing and stability of the miRNA compared with the mRNA as well as the fact that transcription at the *Pank3* locus has to triple in order to lead to doubling in the mature miR-103 production due to very similar basal expression levels of the two miR-103 loci (data not shown, see also 'Discussion' section).

Unlike for miR-103, the initial induction of miR-148b slightly preceded that of its host gene *Copz1* and showed a peak after D6 of differentiation (Figure 2D). Both miR-148b and its host gene *Copz1* were upregulated more moderately than the other tested PPARγ target genes and for *Copz1* (and the pri-miR-148b) the fold change never exceeded 3-fold. The upregulation of miR-96 was fairly robust reaching maximum induction around D8 of differentiation and resembling the delayed induction of miR-103 (Figure 2E). However, the expression profile of pri-miR-96 suggests that the locus is transcriptionally activated already at earlier stages of differentiation.

By far the most induced of all the tested miRNAs was miR-205 that had strongly increased already on D3 of differentiation and reached several hundred-fold induction by the end of the differentiation (Figure 2F). The extent of the induction can be explained by the very low basal expression of miR-205 in pre-adipocytes (data not shown). Similarly to the mature miRNA, also pri-miR-205 was upregulated during the time course, although with lower fold change. This argues that increased transcriptional activity at the miR-205 locus is contributing to the robust observed induction of the mature miRNA, while specific regulation of the miRNA biogenesis pathway might also play a role.

The upregulation of miR-378 was the second highest of all the miRNAs tested (Figure 2G). The host gene of miR-378, *Ppargc1b*, encodes for PGC-1β, which is an important transcriptional co-activator of PPARγ as well as other transcription factors (30,31). *Ppargc1b* expression was induced already early on with a very similar profile to known PPARγ target genes, followed by strong increase in pri-miR-378. The mature miR-378 followed the expression of the host gene and the primary transcript, leading again to slightly delayed response by the mature miRNA.

In general, the pri-miRNAs showed quite different dynamics from their respective mature miRNAs, and especially for miR-205, these inductions were clearly weaker. These differences may be explained by the relatively low stability of the transient pri-miRNA transcripts that are processed into pre-miRNAs co-transcriptionally (32,33). To address this possibility in more detail we specifically inhibited RNA Pol II-mediated transcriptional elongation in D6 adipocytes by treating the cells with DRB for a time course of 12, 24 and 48 h (Supplementary Figure S3A). As expected, all tested mRNAs had decreased by around 50% or more already after 12 h and remained at lowered levels throughout the treatment (Supplementary Figure S3B–G). *Cebpa* and *Pparg* were the least stable mRNAs with only 5–20% of the transcripts remaining after DRB treatment when compared with cells similarly treated with the DMSO vehicle (Supplementary Figure S3B). Similarly to mRNAs, the pri-miRNA transcripts were all reduced up to 10-fold after 12 h of transcription inhibition and for all except pri-miR-103-2 remained below the control levels (Supplementary Figure S3B–G). Curiously, all pri-miRNA transcripts exhibited some increase in their levels towards the end of the treatment. This might to be explained by decreased processing of the primary transcripts upon prolonged inhibition of RNA Pol II. In contrast to the unstable pri-miRNA transcripts, most of

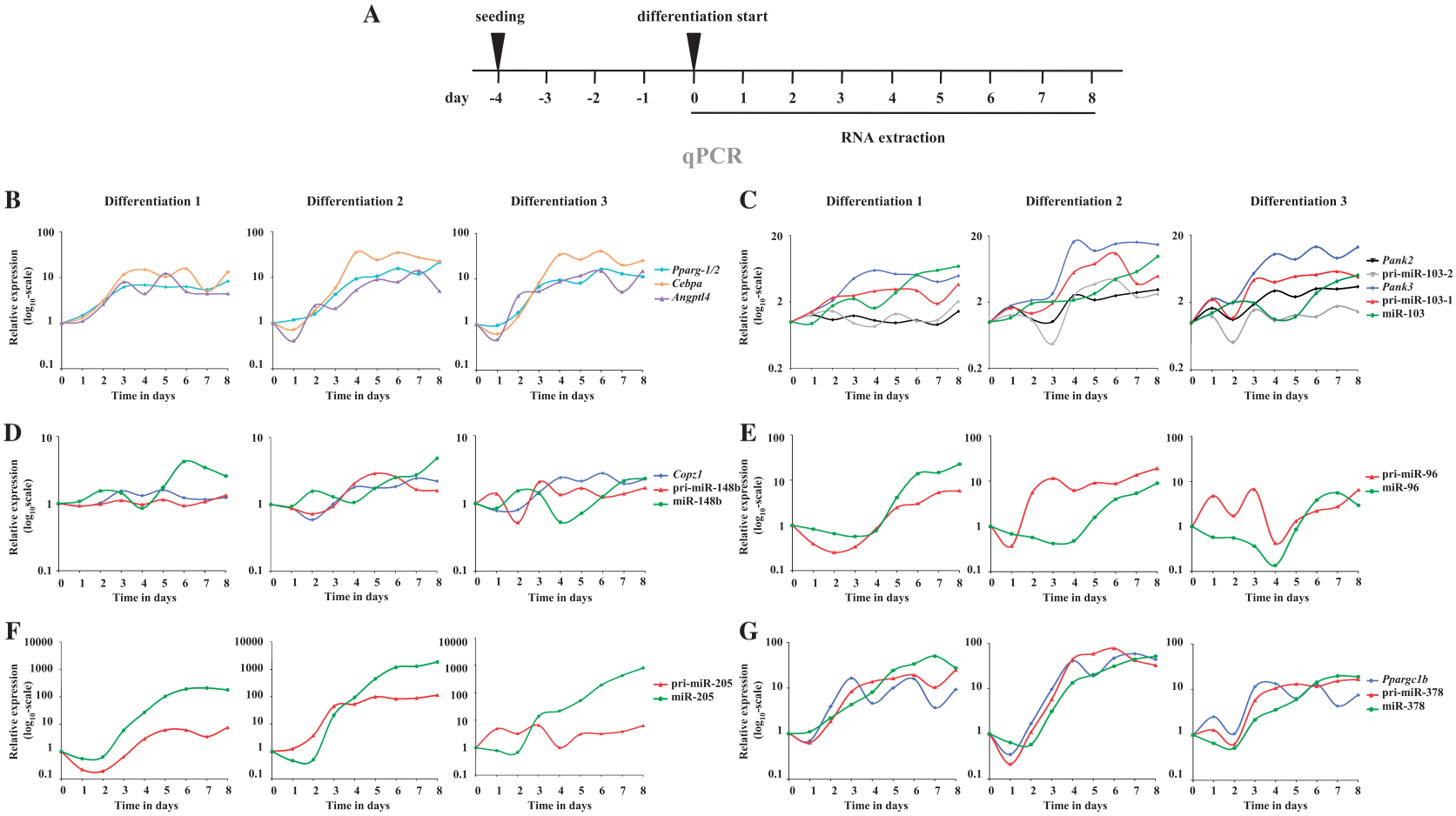

Figure 2. Expression profiles of the candidate PPARγ target miRNAs and host genes during 8 days of 3T3-L1 mouse pre-adipocyte differentiation. qPCR with gene-specific primers for miRNA host genes and the pri-miRNAs or TaqMan probes for the mature miRNAs were used to measure the expression profiles of the different transcripts during 8 days of 3T3-L1 mouse pre-adipocyte differentiation. Schematic depictions of the locations of qPCR primers are provided in Supplementary Figure S1 (**A**) Schematic representation of the differentiation procedure and the collection time points. (**B–G**) Individual panels depict the relative expression profiles during adipogenesis in three independent differentiation experiments (Differentiation 1–3) for (B) *Pparg*, *Angptl4* and *Cebpa*; (C) *Pank2*, *Pank3*, pri-miR-103-1, pri-miR-103-2 and the mature miR-103; (D) *Copz1*, pri-miR-148b and miR-148b; (E) pri-miR-96 and miR-96; (F) pri-miR-205 and miR-205 and (G) *Ppargc1b*, pri-miR-378 and miR-378. The measured expression values were normalized to *Rpl13a* mRNA (for mRNAs and pri-miRNAs) or U6 small nuclear RNA (snRNA) (for miRNAs) and are shown relative to D0. The results from three independent differentiation experiments are shown. The statistical significance of the changes for each transcript during the time course of the three independent differentiations was tested using ANOVA. All tested mRNAs, all mature miRNAs except miR-148b and pri-miR transcripts for miR-103-1, miR-205 and miR-378 were significantly affected during differentiation ($P < 0.05$; for pri-miR-96 the P-value was 0.078).

the mature miRNAs remained unaffected throughout the experiments and only miRNAs miR-205 and miR-378 decreased clearly below the DMSO-control levels after 48 h of DRB treatment (Supplementary Figure S3F and G). These results are consistent with previous studies suggesting high stability of mature miRNA transcripts (34,35) and readily explain the observed differences in the expression profiles of the pri-miRNAs and their mature counterparts.

Taken together, five candidate PPARγ target miRNAs were dynamically upregulated during 3T3-L1 differentiation, most likely due to increased transcription at their genomic loci as indicated by the induced levels of the respective pri-miRNA transcripts. With the exception of miR-103-2, the expression of all tested genes followed that of *Pparg*, implicating them as possible primary PPARγ target genes.

PPARγ-dependence of the candidate PPARγ-target miRNAs and their host genes

To test the PPARγ-dependence of the candidate PPARγ target miRNA genes, we performed siRNA silencing of PPARγ on D6 of 3T3-L1 differentiation (Figure 3A). At 48 h post-transfection the expression of both PPARγ variants had strongly decreased on the protein level (Supplementary Figure S4) and the *Pparg* mRNA level was reduced below 30% of that in cells transfected with an unspecific control siRNA (Figure 3B). The expression levels of the two primary PPARγ target genes, *Cebpa* and *Angptl4*, were also decreased, confirming a reduced transcriptional activation by PPARγ.

Comparison of the two miR-103 loci showed that pri-miR-103-1 and especially its host gene *Pank3* were downregulated by PPARγ silencing, while pri-miR-103-2 and its host gene *Pank2* were not affected (Figure 3C). This also further confirms miR-103-1 as the main source of miR-103 upregulation during adipogenesis. However, reduction in the levels of mature miR-103 could not be detected yet at this point, most likely due to remarkably high stability of the mature miRNA (Supplementary Figure S3). Consistent with their moderate induction in adipogenesis, mature miR-148b and pri-miR-148b remained mainly unaffected by PPARγ silencing, and their host gene *Copz1* was only modestly, although significantly, downregulated (Figure 3D). Pri-miR-96 was decreased to same extent as the mature miR-96 (Figure 3E). Similarly, both pri-miR-205 and miR-205, which were the two most strongly affected miRNA transcripts tested, showed a drastic reduction down to 20–30% of their expression level (Figure 3F). Finally, pri-miR-378, mature miR-378 and their host gene *Ppargc1b* were all significantly downregulated by PPARγ silencing (Figure 3G).

In summary, all candidate PPARγ-targeted miRNA loci except miR-148b and miR-103-2 depend on PPARγ for their expression in mouse adipocytes. Moreover, this dependence can be attributed to their transcriptional regulation as demonstrated by the reduced levels of the respective pri-miRNA transcripts and host genes.

Effects of RGZ on candidate PPARγ target miRNAs and their host genes

One classical approach to identify primary target genes of ligand-dependent nuclear receptors includes short-time treatments with agonists. Therefore, we tested treatments of differentiating 3T3-L1 cells at D2, D4 and D6 with the PPARγ agonist RGZ and observed highest upregulation of the known primary PPARγ target genes *Cebpa* and *Angptl4* at D2 (Figure 4A and B and data not shown). This is an obvious time point for RGZ treatment, since on D2 the levels of PPARγ expression have already increased but the cells have not yet been exposed to RGZ or high levels of endogenous ligands. To test the RGZ response of the candidate genes we performed a time series of RGZ treatments and collected RNA 4, 8, 12, 24 and 48 h after the treatment (Figure 4A). In agreement with around 24-h delay in the upregulation of mature miRNAs observed during the differentiation time course (Figure 2), the mature miR-378 was not induced until after 12 h of RGZ treatment and the more stable miR-103 became induced only after 48 h (Figures 4C–G). In contrast miR-205 was significantly induced already 4 h after RGZ treatment, reached almost 3-fold induction by 8 h and continued to accumulate up to 10-fold by 48 h (Figure 4F). Consistently, also pri-miR-205 showed a clear response to the agonist treatment, although with a weaker fold change. Likewise, pri-miR-103-1 and pri-miR-378 were both significantly induced upon PPARγ activation and continued to accumulate throughout the time course (Figure 4C and G), while inductions of pri-miR-148b and pri-miR-96 as well as their mature counterparts were either very weak or not significant (Figure 4D and E). Similarly to the pri-miRNAs, the host genes of miR-103-1 and miR-378, *Pank3* and *Pparg1b*, were also significantly upregulated already after first time points of RGZ treatment, arguing that these genes are indeed primary PPARγ targets.

Taken together, from the six candidate PPARγ target miRNA genes three, namely miR-103-1, miR-205 and miR-378, and the two host genes *Pank3* and *Ppargc1b* could be confirmed as PPARγ targets also by upregulation upon treatment with the PPARγ ligand RGZ.

Validation of the PPARγ association with PPREs on the *Pank3*, *Ppargc1b* and miR-205 loci

In order to validate direct binding of PPARγ to the regulatory regions of our newly identified PPARγ target genes, we performed regular ChIP assays followed by qPCR with chromatin extracted from 3T3-L1 cells at D0 and D6 expressing either low or high levels of PPARγ (Figure 5, Supplementary Figure S4). In order to confirm that the observed enrichments are specific for PPARγ, we used two different PPARγ antibodies in separate immunoprecipitations (one used in the previous genome-wide studies and another independent antibody from a different provider, see 'Materials and Methods' section). For this validation we focused our efforts on the three miRNA loci that were most responsive to RGZ, namely miR-103-1, miR-205 and miR-378. As positive control we used the known PPARγ target gene *Angptl4* and as negative

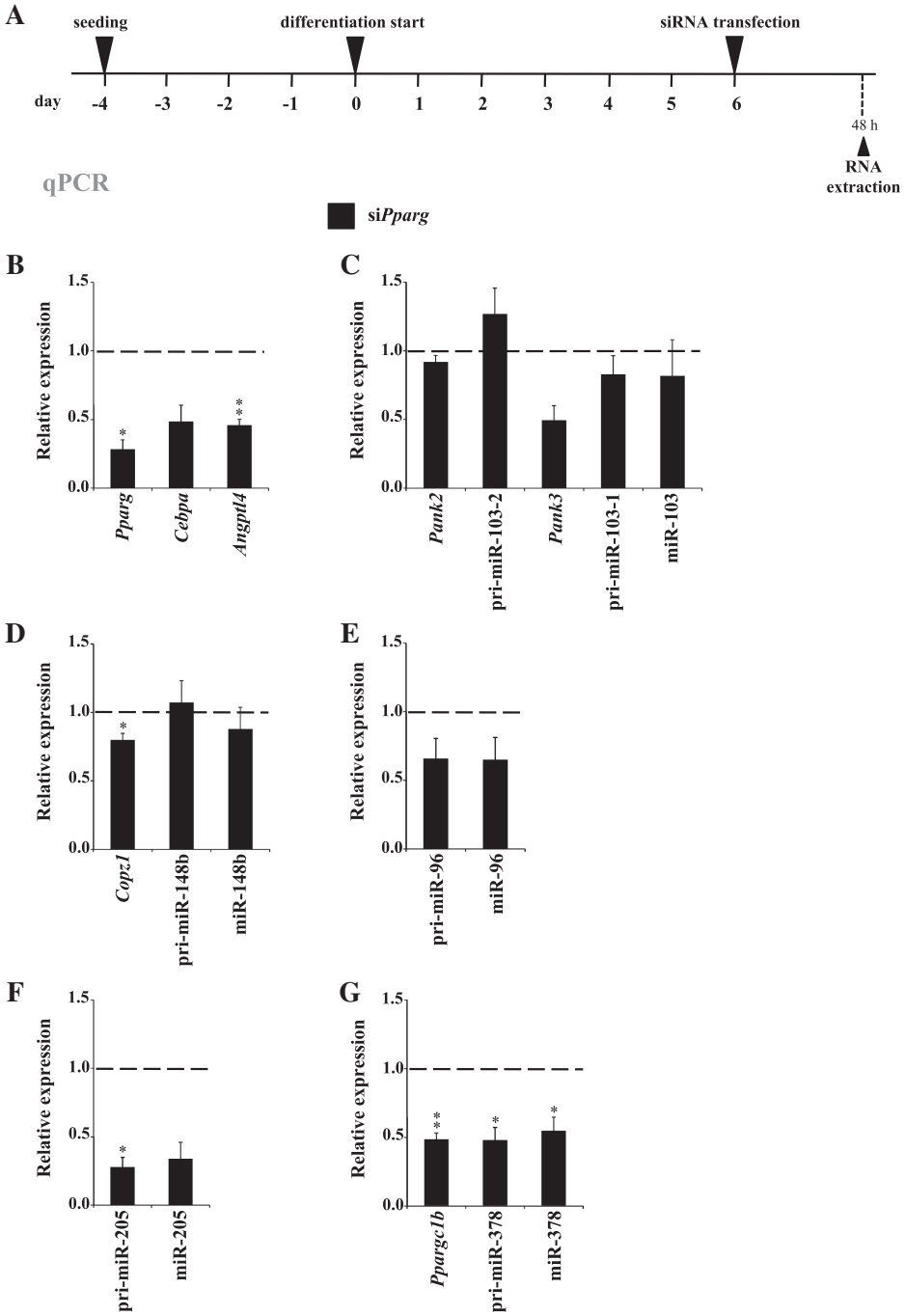

Figure 3. Effects of PPARγ downregulation in mature mouse 3T3-L1 adipocytes on the candidate miRNAs and their host genes. (**A**) Schematic representation of the experimental procedure for silencing PPARγ in differentiated 3T3-L1 adipocytes. Six days differentiated 3T3-L1 cells were transfected with siRNA specific for *Pparg* (si*Pparg*) or with unspecific control siRNA (si*Control)*. Forty-eight hours post-transfection the cells were collected and the total RNA was extracted. (B–G) qPCR analysis of the relative expression values in si*Pparg* transfected cells compared with si*Control* transfection for (**B**) *Pparg, Cebpa* and *Angptl4*; (**C**) *Pank2*, *Pank3*, pri-miR-103-1, pri-miR-103-2 and miR-103; (**D**) *Copz1*, pri-miR-148b and miR-148b; (**E**) pri-miR-96 and miR-96; (**F**) pri-miR-205 and miR-205 and (**G**) *Ppargc1b*, pri-miR-378 and miR-378. The measured expression values were normalized to *Rpl13a* mRNA (for mRNAs and pri-miRNAs) or U6 snRNA (for miRNAs) and are shown relative to si*Control*, value of which was set to 1 (indicated by dashed line). Data points indicate the mean expression values of four independent experiments and the error bars represent SEM. One sample *t*-test was performed to determine the significance of downregulation upon si*Pparg* transfection (*$P < 0.05$; **$P < 0.01$; for *Cebpa*, *Pank3*, pri-miR-96, miR-96 and miR-205 the *P*-values of downregulation were 0.096, 0.078, 0.097, 0.139 and 0.052, respectively).

control the *Pou5f1* gene, which is not significantly expressed in adipocytes (data not shown). Examination of the genomic regions ±100 kb from the TSS of *Angptl4* (Figure 5A), *Pou5f1* (Figure 5B), *Pank3* (miR-103-1) (Figure 5C) and *Ppargc1b* (miR-378) (Figure 5D), and ±120 kb from the TSS of miR-205 (Figure 5E) identified 8, 2, 10, 13 and 5 independent PPARγ-bound sites on each locus, respectively, when

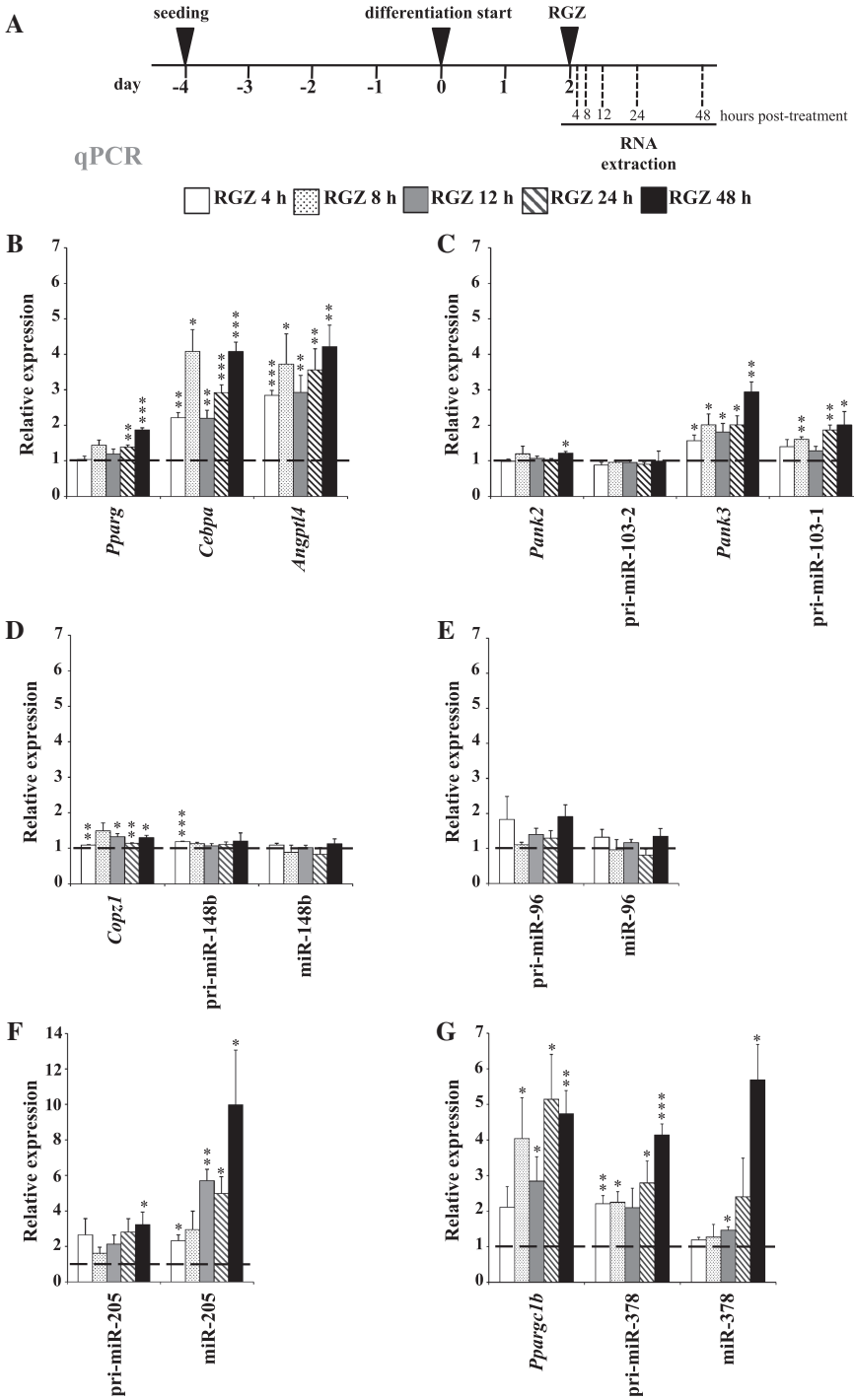

Figure 4. Effects of RGZ treatment of 2 days differentiated 3T3-L1 cells on the candidate miRNAs and their host genes. (**A**) Experimental procedure for RGZ treatment of 2 days differentiated 3T3-L1 cells. (**B–G**) qPCR analysis of the relative expression values in RGZ-treated cells compared with DMSO-treated controls for (B) *Pparg, Cebpa* and *Angptl4*; (C) *Pank2*, *Pank3*, pri-miR-103-1, pri-miR-103-2 and miR-103; (D) *Copz1*, pri-miR-148b and miR-148b; (E) pri-miR-96 and miR-96; (F) pri-miR-205 and miR-205 and (G) *Ppargc1b*, pri-miR-378 and miR-378. The measured expression values were normalized to *Rpl13a* mRNA (for mRNAs and pri-miRNAs) or U6 snRNA (for miRNAs) and are shown relative to DMSO treatment, value of which was set to 1 (indicated by dashed line). Data points indicate the mean expression values of at least three independent experiments and the error bars represent SEM. One sample *t*-test was performed to determine the significance of upregulation upon RGZ treatment (*$P < 0.05$; **$P < 0.01$; ***$P < 0.001$).

looking at all four genome-wide datasets. To identify the PPARγ-bound sites that could correspond to direct DNA binding of PPARγ to a PPRE, we aligned the ChIP-identified binding sites with PPREs predicted by the REsearch algorithm (10). Predictions by REsearch are based on PPARγ binding in gel shift analysis and, in addition to the PPRE location, provide information about the strength of the PPARγ–PPRE interaction

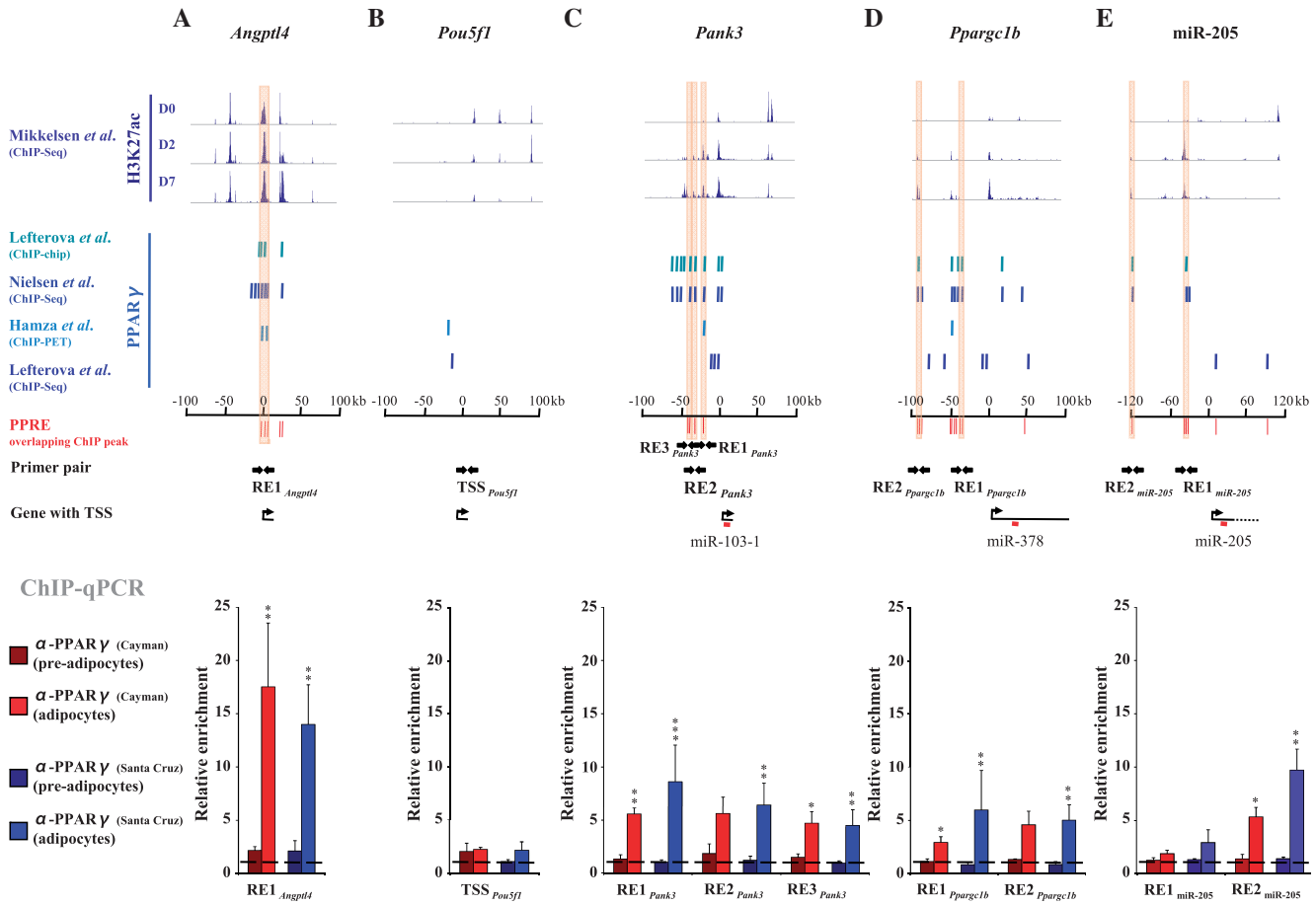

Figure 5. Identification of active PPREs responsible for direct PPARγ–DNA interaction and validation of the PPARγ binding at the PPREs on the *Pank3*, *Ppargc1b* and miR-205 loci by ChIP analysis. (**A–E**, top panel) Levels of H3K27 acetylation determined by ChIP-Seq (7) at D0, D2 and D7 of 3T3-L1 differentiation and (A–E, middle panel) PPARγ-binding sites determined by ChIP-chip (3), ChIP-Seq (4,6) and ChIP-PET (5) ± 100 kb around the TSS of (A) the *Angptl4* positive control locus, (B) the *Pou5f1* negative control locus, (C) *Pank3* (miR-103-1), (D) *Ppargc1b* (miR-378) and (E) ± 120 kb around the TSS of miR-205. *In silico* predicted PPREs overlapping with the ChIP binding sites are marked in red. The PPREs selected for validation are highlighted and the primers used to amplify regions overlapping these PPREs are indicated as arrows. (A–E, lower panel) ChIP analysis using two different PPARγ antibodies from independent providers [α-PPARγ (Cayman) or α-PPARγ (Santa-Cruz)] and IgG as a control. qPCR was performed with DNA immunoprecipitated from pre-adipocytes (D0) or adipocytes (D6) and using primers specific for (A) a known PPRE on the *Angptl4* locus, (B) an unrelated control region on the *Pou5f1* locus, (C) three putative PPREs ($RE1_{Pank3}$, $RE2_{Pank3}$ and $RE3_{Pank3}$) on the *Pank3* locus, (D) two clusters of putative PPREs ($RE1_{Ppargc1b}$ and $RE2_{Ppargc1b}$) on the *Ppargc1b* locus and two putative PPREs ($RE1_{miR205}$ and $RE2_{miR205}$) on the miR-205 locus. The measured enrichment values were normalized to 1:100 diluted input DNA. The enrichment of PPARγ is shown relative to the enrichment of IgG (indicated by dashed line). Data points indicate the mean enrichment values of at least three independent experiments and the error bars represent SEM. One sample *t*-test was performed to determine the significance of PPARγ enrichment at D6 compared with D0 (*$P < 0.05$; **$P < 0.01$; ***$P < 0.001$).

in vitro. This filtering approach reduced the number of genomic regions to two for *Angptl4*, none for *Pou5f1*, three for *Pank3* and five for both *Ppargc1b* and miR-205. For the *Angptl4* gene we selected $RE1_{Angptl4}$ containing three predicted PPREs, one of which is a known functional PPRE in adipocytes (28). For the *Pou5f1* gene we used its TSS region (TSS_{Pou5f1}). The three PPREs, $RE1_{Pank3}$, $RE2_{Pank3}$ and $RE3_{Pank3}$, are located ~19, 31 and 37 kb upstream from the *Pank3* TSS, respectively. $RE3_{Pank3}$ in fact contains two separate PPREs located within 200 bp from each other. All three REs contain PPREs with good *in vitro* binding strength for PPARγ. From the five PPARγ-bound sites of the *Ppargc1b* locus four contain at least two adjacent PPREs each. Two of them, $RE1_{Ppargc1b}$ and $RE2_{Ppargc1b}$, located ~38 and 90 kb upstream from *Ppargc1b* TSS, were selected for validation. $RE2_{Ppargc1b}$ contains two strong PPREs and one weak PPRE while $RE1_{Ppargc1b}$ has only two weak PPREs. Finally, from the five PPARγ-bound sites at miR-205 locus we chose two, $RE1_{miR-205}$ and $RE2_{miR-205}$, to be validated. The sites are located at 37 and 118 kb upstream from the miR-205 TSS with one PPRE in each. The sequences and the exact locations of the PPREs are provided in Supplementary Table S5.

In ChIP assays PPARγ showed low association with $RE1_{Angptl4}$ in pre-adipocytes (D0) but in differentiated adipocytes (D6) a significant increase in enrichment to ~15-fold over IgG could be observed at this genomic region with both PPARγ antibodies (Figure 5A), reflecting the specific binding by PPARγ during differentiation. The enrichment of the control TSS_{Pou5f1} remained at the background level in both conditions (Figure 5B). Importantly,

the enrichments of the three REs at the *Pank3* locus (Figure 5C), the two tested REs at the *Ppargc1b* locus (Figure 5D) as well as $RE2_{miR\text{-}205}$ (Figure 5E) all exhibited strong and mostly significant increases in their enrichments between pre-adipocytes and adipocytes. Finally, all enrichments were consistent between the two antibodies, arguing that we are monitoring specific binding of PPARγ at these regions.

Since the interaction of PPARγ with the selected REs could be validated by regular ChIP assays, we were interested to see whether these regions could indeed be active enhancers contributing to regulation of expression of the confirmed target genes. To address this possibility, we took advantage of the recent identification of acetylation of lysine 27 of histone H3 (H3K27ac) as a histone modification specifically marking active enhancer regions (36,37). Analysis of the published ChIP-Seq data from Mikkelsen *et al.* (7) for the level of H3K27ac at our loci of interest during 3T3-L1 differentiation confirmed that all of our tested REs, except $RE3_{Pank3}$, are accumulating H3K27 acetylation during adipogenesis (Figure 5, top panel). These data argue that the identified PPREs can serve as specific binding sites for PPARγ during adipogenesis and contribute as active enhancers to the regulation of the identified primary PPARγ target miRNA genes.

DISCUSSION

This study was performed with the aim to identify miRNA genes that are primary nuclear receptor targets. Since miRNA genes often serve as critical developmental switches and are regulated in differentiation processes (23), we have chosen adipogenesis as an experimental system, where a dominant role is played by the nuclear receptor PPARγ (2). We selected the mouse 3T3-L1 cells as a cellular model, for which far more public data are available than for any comparable human system (3–6,26). Our approach for the identification of miRNA genes that are primary PPARγ targets was to integrate genome-wide data about PPARγ binding with recent information on TSS locations of miRNA genes.

Although the genome-wide PPARγ location data were obtained with the same cellular model and the same antibody, we realized that only the minority of the PPARγ-bound sites are confirmed in at least three of the four datasets. The integration of the four datasets suggested that for 140 miRNAs a PPARγ-bound site is located within 50-kb distance from their TSS in at least one of the datasets. Since PPARγ is significantly upregulated during adipogenesis, a filtering of the 140 miRNAs for those that are more than 2-fold upregulated during 3T3-L1 differentiation, reduced the number to 19 miRNAs encoded by 22 miRNA genes that form the list of putative PPARγ targets. However, the condition that PPARγ binding at the genomic region had to be confirmed in at least three of the four datasets, reduced the list to six miRNA genes miR-103-1, miR-103-2, miR-148b, miR-183/96/182, miR-205 and miR-378. Both a detailed time course analysis of the upregulation of these miRNAs as well as PPARγ silencing in differentiated adipocytes excluded only miR-103-2 and miR-148b from this list of putative primary PPARγ target genes. Still, PPARγ might influence also the transcription of miR-103-2 and miR-148b loci, although not as potently as for the other tested loci, or for example in a different cellular context. Importantly, the genes encoding miR-103-1, miR-205 and miR-378 could be confirmed as classical PPARγ targets also by RGZ treatments. Interestingly, the host genes of these miRNAs, *Pank3* and *Ppargc1b,* are also primary PPARγ target genes, which have not yet been reported as such. For *Pank3* (miR-103-1) we validated three genomic PPARγ binding sites that overlap with *in silico* predicted PPREs 19, 31 and 37 kb upstream from the *Pank3* TSS, for the *Ppargc1b* (miR-378) locus two PPARγ locations with adjacent PPREs 90 and 38kb upstream of the TSS, and for the miR-205 locus one PPARγ binding site with PPRE at 118-kb upstream of the TSS. The future work to identify the exact PPRE sequences responsible for target gene regulation, especially for REs containing multiple PPREs, will require detailed experiments applying reporter gene assays or optimally zinc-finger nuclease-mediated targeting of individual endogenous PPREs. However, by applying the genome-wide mapping of H3K27ac, a histone modification specifically marking the active enhancer regions, we have already shown that most of the validated PPARγ-bound sites are accumulating increased levels of H3K27ac, suggesting that these enhancers are actively contributing to the regulation of the identified target genes.

Since Lefterova *et al.* (3) have shown PPARγ to co-localize with the transcription factor CEBPα in differentiated 3T3-L1 cells, we took advantage of this dataset and compared CEBPα-bound sites with the PPARγ-bound sites at miRNA loci. In most of them (29 of the 52) CEBPα was found in <1 kb distance from the respective PPARγ-bound sites (data not shown). Moreover, all of the six candidate miRNA loci except miR-205 had their regulatory regions co-occupied by PPARγ and CEBPα, suggesting that the two transcription factors might induce different miRNA genes in a combinatorial manner, similarly to protein coding genes (data not shown) (3).

Although most of our candidate miRNA genes depend on PPARγ for their expression in adipocytes, we found that the dynamics of their expression changes, and those of their host genes, varied during adipogenesis. This is perhaps most evident for miR-103, which exhibits a delay in its upregulation when compared with the host gene *Pank3*. While this observation might be mainly explained by different processing of the two mature transcripts, the usage of alternative TSSs or differential stability of the two mature transcripts could also play a role. Histone H3 lysine 4 trimethylation (H3K4me3) is an epigenetic modification known to mark active TSSs. Based on genome-wide mapping of H3K4me3 in mouse 3T3-L1 cells, only one TSS exists at the *Pank3* locus during adipogenesis (7). This argues that the differences observed in the expression dynamics are more likely to be explained by the dissimilar stabilities of the mature transcripts, rather than alternative TSS usage. Indeed,

consistently with our observations (Supplementary Figure S3), miRNAs were recently estimated to possess an average half-life of almost 5 days (35). This is 12 times longer than the median half-life of mRNAs, which is 10 h (38). When a mature transcript exhibits a low turnover, it accumulates higher basal expression levels, even upon low levels of basal transcription. Consequently, upon increased expression such transcript can exhibit relatively low fold inductions with slower accumulation rate although the extent of transcriptional output is comparable with that of a lower stability transcript. Therefore, it is likely that the different dynamics of miR-103 (and other miRNAs) are explained by its higher stability compared with the mature *Pank3* mRNA (Supplementary Figure S3). Consistently, we found that 48 h knock-down of PPARγ had no significant effects on mature miR-103 and its response to treatments with RGZ occurred only after 48 h, while the host gene *Pank3* clearly responded already after 4 h.

Transcriptional regulation by PPARγ is both necessary and sufficient for adipogenesis and therefore its primary target genes, including the miRNA genes described here, might play a critical role or at least contribute to successful adipogenesis. Indeed, miR-103 has already been described as highly induced in primary mouse adipocytes and as capable of accelerating adipogenesis (26). miR-103 belongs to a family of three miRNAs, miR-103-1, miR-103-2 and miR-107, that have almost identical sequences and are transcribed together with their host genes *Pank3*, *Pank2* and *Pank1*, respectively (22,29). Interestingly, in addition to the two miR-103 loci also miR-107 was identified as a putative PPARγ target gene in our initial analysis (Figure 1A) and its host gene *Pank1* has been described as a primary PPARα target in human liver (39). Importantly, recent data from Trajkovski *et al.* (40) demonstrated that silencing of miR-103 and miR-107 in the adipose tissue of mice leads to reduced fat levels, but in contradiction to previous *in vitro* data, not via inhibition of adipogenesis. Instead, lowered levels of the miRNAs increased the insulin sensitivity of the adipocytes, a phenomenon linked to increased number of smaller sized adipocytes. Therefore, our data, together with abovementioned findings, create direct links between PPARs, miR-103/107 family miRNAs and insulin sensitivity.

Unlike miR-103, the miR-183/96/182 cluster has not been functionally connected to adipogenesis so far. However, based on the very robust induction that we observed during 3T3-L1 adipogenesis, the members of this cluster are likely to contribute to the biology of mature adipocytes. Treatment with insulin alone was recently shown to downregulate miR-183 levels in 3T3-L1 adipocytes (41). However, during adipogenesis the cluster becomes upregulated in a PPARγ-dependent manner, despite the presence of insulin in the differentiation medium. Therefore, it is probable that the expression of the miR-183/96/182 cluster is under combinatorial regulation of several transcription factors and pathways that together lead to the clusters increased expression in adipocytes.

By far the highest induced miRNA tested in our analysis was miR-205. The exact significance of this induction for adipogenesis remains unclear for now. However, the list of predicted target mRNAs for miR-205 includes, for example, *Runx2* (TargetScan 5.2), a transcript encoding a transcription factor with an important role in favoring osteoblastogenesis over adipogenesis during mesenchymal stem cell differentiation (42). High levels of PPARγ are known to suppress RUNX2 protein expression and induction of miR-205 might serve as a mechanism to achieve this suppression. Indeed, Zhang *et al.* (43) recently showed that miR-205 can attenuate RUNX2 protein accumulation together with nine other miRNAs in mouse osteoblasts. However, our preliminary experiments have so far failed to demonstrate reduction in *Runx2* mRNA levels upon miR-205 overexpression in pre-adipocytes (data not shown), suggesting that a combinatorial function of multiple miRNAs might be required for robust regulation of *Runx2* at the mRNA level. Consistently, we were so far unable to demonstrate any significant impact of miR-205 overexpression on early adipogenesis in general, as measured by the expression levels of the known adipocyte marker genes such as *Pparg* and *Cebpa* (data not shown). Proteome- or transcriptome-wide analysis upon gain- or loss-of-function of miR-205 would be needed to reveal the primary targets mRNAs and pathways regulated by the robust induction of miR-205 during adipogenesis.

Interestingly, we also found miR-378 and its host gene *Ppargc1b* as primary PPARγ targets in adipocytes. miR-378 can induce lipogenesis and expression of lipogenic genes, when overexpressed during adipogenesis of ST2 mesenchymal precursors (44). Moreover, *Ppargc1b* is a known transcriptional co-activator responsible for inducing the target genes of numerous transcription factors (for example, sterol response element binding proteins, liver X receptors and PPARs) that are involved in regulation of lipogenesis and related processes (31). This suggests that PPARγ may induce both miR-378 and *Ppargc1b*, in order to allow both to function synergistically in the regulation of lipid metabolism. Importantly, this induction is not limited to mouse 3T3-L1 cells as miR-378 was recently identified as the most highly upregulated miRNA during the differentiation of both mouse and human primary adipocytes (26,45).

In addition to miRNAs discussed above, a more detailed analysis of our initial list of putative PPARγ target miRNA genes will lead to a more complete list of the true PPARγ target miRNAs. Revealing the role of these miRNAs in adipogenesis and identification of their primary target mRNAs will be important for their integration to the regulatory networks governing adipogenesis.

SUPPLEMENTARY DATA

Supplementary Data are available at NAR Online: Supplementary Tables S1–S5 and Supplementary Figures S1–S4.

FUNDING

University of Luxembourg, National Research Fund (FNR, Luxembourg), Televie (FNRS, Belgium, to C.C.); fellowships from the National Research Fund (FNR, Luxembourg to E.J. and M.L.). Funding for open access charge: University of Luxembourg.

Conflict of interest statement. None declared.

REFERENCES

1. Farmer,S.R. (2006) Transcriptional control of adipocyte formation. *Cell Metab.*, **4**, 263–273.
2. Rosen,E.D., Sarraf,P., Troy,A.E., Bradwin,G., Moore,K., Milstone,D.S., Spiegelman,B.M. and Mortensen,R.M. (1999) PPAR gamma is required for the differentiation of adipose tissue in vivo and in vitro. *Mol. Cell*, **4**, 611–617.
3. Lefterova,M.I., Zhang,Y., Steger,D.J., Schupp,M., Schug,J., Cristancho,A., Feng,D., Zhuo,D., Stoeckert,C.J. Jr, Liu,X.S. *et al.* (2008) PPARgamma and C/EBP factors orchestrate adipocyte biology via adjacent binding on a genome-wide scale. *Genes Dev.*, **22**, 2941–2952.
4. Nielsen,R., Pedersen,T.A., Hagenbeek,D., Moulos,P., Siersbaek,R., Megens,E., Denissov,S., Borgesen,M., Francoijs,K.J., Mandrup,S. *et al.* (2008) Genome-wide profiling of PPARgamma:RXR and RNA polymerase II occupancy reveals temporal activation of distinct metabolic pathways and changes in RXR dimer composition during adipogenesis. *Genes Dev.*, **22**, 2953–2967.
5. Hamza,M.S., Pott,S., Vega,V.B., Thomsen,J.S., Kandhadayar,G.S., Ng,P.W., Chiu,K.P., Pettersson,S., Wei,C.L., Ruan,Y. *et al.* (2009) De-novo identification of PPARgamma/RXR binding sites and direct targets during adipogenesis. *PLoS One*, **4**, e4907.
6. Lefterova,M.I., Steger,D.J., Zhuo,D., Qatanani,M., Mullican,S.E., Tuteja,G., Manduchi,E., Grant,G.R. and Lazar,M.A. (2010) Cell-specific determinants of peroxisome proliferator-activated receptor gamma function in adipocytes and macrophages. *Mol. Cell. Biol.*, **30**, 2078–2089.
7. Mikkelsen,T.S., Xu,Z., Zhang,X., Wang,L., Gimble,J.M., Lander,E.S. and Rosen,E.D. (2010) Comparative epigenomic analysis of murine and human adipogenesis. *Cell*, **143**, 156–169.
8. Diamant,M. and Heine,R.J. (2003) Thiazolidinediones in type 2 diabetes mellitus: current clinical evidence. *Drugs*, **63**, 1373–1405.
9. Heinäniemi,M. and Carlberg,C. (2008) Screening for PPAR responsive regulatory modules in cancer. *PPAR Res.*, **2008**, 749073.
10. Heinäniemi,M., Uski,J.O., Degenhardt,T. and Carlberg,C. (2007) Meta-analysis of primary target genes of peroxisome proliferator-activated receptors. *Genome Biol.*, **8**, R147.
11. Kliewer,S.A., Umesono,K., Noonan,D.J., Heyman,R.A. and Evans,R.M. (1992) Convergence of 9-cis retinoic acid and peroxisome proliferator signalling pathways through heterodimer formation of their receptors. *Nature*, **358**, 771–774.
12. Glass,C.K. and Saijo,K. (2010) Nuclear receptor transrepression pathways that regulate inflammation in macrophages and T cells. *Nat. Rev. Immunol.*, **10**, 365–376.
13. Han,L., Zhou,R., Niu,J., McNutt,M.A., Wang,P. and Tong,T. (2010) SIRT1 is regulated by a PPAR{gamma}-SIRT1 negative feedback loop associated with senescence. *Nucleic Acids Res.*, **38**, 7458–7471.
14. Ghildiyal,M. and Zamore,P.D. (2009) Small silencing RNAs: an expanding universe. *Nat. Rev. Genet.*, **10**, 94–108.
15. Kim,V.N. (2005) MicroRNA biogenesis: coordinated cropping and dicing. *Nat. Rev. Mol. Cell. Biol.*, **6**, 376–385.
16. Valencia-Sanchez,M.A., Liu,J., Hannon,G.J. and Parker,R. (2006) Control of translation and mRNA degradation by miRNAs and siRNAs. *Genes Dev.*, **20**, 515–524.
17. Guo,H., Ingolia,N.T., Weissman,J.S. and Bartel,D.P. (2010) Mammalian microRNAs predominantly act to decrease target mRNA levels. *Nature*, **466**, 835–840.
18. Selbach,M., Schwanhausser,B., Thierfelder,N., Fang,Z., Khanin,R. and Rajewsky,N. (2008) Widespread changes in protein synthesis induced by microRNAs. *Nature*, **455**, 58–63.
19. Farh,K.K., Grimson,A., Jan,C., Lewis,B.P., Johnston,W.K., Lim,L.P., Burge,C.B. and Bartel,D.P. (2005) The widespread impact of mammalian MicroRNAs on mRNA repression and evolution. *Science*, **310**, 1817–1821.
20. Sinkkonen,L., Hugenschmidt,T., Berninger,P., Gaidatzis,D., Mohn,F., Artus-Revel,C.G., Zavolan,M., Svoboda,P. and Filipowicz,W. (2008) MicroRNAs control de novo DNA methylation through regulation of transcriptional repressors in mouse embryonic stem cells. *Nat. Struct. Mol. Biol.*, **15**, 259–267.
21. Marson,A., Levine,S.S., Cole,M.F., Frampton,G.M., Brambrink,T., Johnstone,S., Guenther,M.G., Johnston,W.K., Wernig,M., Newman,J. *et al.* (2008) Connecting microRNA genes to the core transcriptional regulatory circuitry of embryonic stem cells. *Cell*, **134**, 521–533.
22. Ozsolak,F., Poling,L.L., Wang,Z., Liu,H., Liu,X.S., Roeder,R.G., Zhang,X., Song,J.S. and Fisher,D.E. (2008) Chromatin structure analyses identify miRNA promoters. *Genes Dev.*, **22**, 3172–3183.
23. Bushati,N. and Cohen,S.M. (2007) microRNA functions. *Annu. Rev. Cell Dev. Biol.*, **23**, 175–205.
24. Mudhasani,R., Puri,V., Hoover,K., Czech,M.P., Imbalzano,A.N. and Jones,S.N. (2010) Dicer is required for the formation of white but not brown adipose tissue. *J. Cell Physiol.*, **226**, 1399–1406.
25. Wang,Q., Li,Y.C., Wang,J., Kong,J., Qi,Y., Quigg,R.J. and Li,X. (2008) miR-17–92 cluster accelerates adipocyte differentiation by negatively regulating tumor-suppressor Rb2/p130. *Proc. Natl Acad. Sci. USA*, **105**, 2889–2894.
26. Xie,H., Lim,B. and Lodish,H.F. (2009) MicroRNAs induced during adipogenesis that accelerate fat cell development are downregulated in obesity. *Diabetes*, **58**, 1050–1057.
27. Hamm,J.K., Park,B.H. and Farmer,S.R. (2001) A role for C/EBPbeta in regulating peroxisome proliferator-activated receptor gamma activity during adipogenesis in 3T3-L1 preadipocytes. *J. Biol. Chem.*, **276**, 18464–18471.
28. Mandard,S., Zandbergen,F., Tan,N.S., Escher,P., Patsouris,D., Koenig,W., Kleemann,R., Bakker,A., Veenman,F., Wahli,W. *et al.* (2004) The direct peroxisome proliferator-activated receptor target fasting-induced adipose factor (FIAF/PGAR/ANGPTL4) is present in blood plasma as a truncated protein that is increased by fenofibrate treatment. *J. Biol. Chem.*, **279**, 34411–34420.
29. Wilfred,B.R., Wang,W.X. and Nelson,P.T. (2007) Energizing miRNA research: a review of the role of miRNAs in lipid metabolism, with a prediction that miR-103/107 regulates human metabolic pathways. *Mol. Genet. Metab.*, **91**, 209–217.
30. Handschin,C. and Spiegelman,B.M. (2006) Peroxisome proliferator-activated receptor gamma coactivator 1 coactivators, energy homeostasis, and metabolism. *Endocr. Rev.*, **27**, 728–735.
31. Lin,J., Handschin,C. and Spiegelman,B.M. (2005) Metabolic control through the PGC-1 family of transcription coactivators. *Cell Metab.*, **1**, 361–370.
32. Morlando,M., Ballarino,M., Gromak,N., Pagano,F., Bozzoni,I. and Proudfoot,N.J. (2008) Primary microRNA transcripts are processed co-transcriptionally. *Nat. Struct. Mol. Biol.*, **15**, 902–909.
33. Pawlicki,J.M. and Steitz,J.A. (2008) Primary microRNA transcript retention at sites of transcription leads to enhanced microRNA production. *J. Cell Biol.*, **182**, 61–76.
34. Bail,S., Swerdel,M., Liu,H., Jiao,X., Goff,L.A., Hart,R.P. and Kiledjian,M. (2010) Differential regulation of microRNA stability. *RNA*, **16**, 1032–1039.
35. Gantier,M.P., McCoy,C.E., Rusinova,I., Saulep,D., Wang,D., Xu,D., Irving,A.T., Behlke,M.A., Hertzog,P.J., Mackay,F. *et al.* (2011) Analysis of microRNA turnover in mammalian cells following Dicer1 ablation. *Nucleic Acids Res.*, **39**, 5692–5703.
36. Creyghton,M.P., Cheng,A.W., Welstead,G.G., Kooistra,T., Carey,B.W., Steine,E.J., Hanna,J., Lodato,M.A., Frampton,G.M., Sharp,P.A. *et al.* (2010) Histone H3K27ac separates active from poised enhancers and predicts developmental state. *Proc. Natl Acad. Sci. USA*, **107**, 21931–21936.
37. Rada-Iglesias,A., Bajpai,R., Swigut,T., Brugmann,S.A., Flynn,R.A. and Wysocka,J. (2011) A unique chromatin signature

uncovers early developmental enhancers in humans. *Nature*, **470**, 279–283.
38. Yang,E., van Nimwegen,E., Zavolan,M., Rajewsky,N., Schroeder,M., Magnasco,M. and Darnell,J.E. Jr (2003) Decay rates of human mRNAs: correlation with functional characteristics and sequence attributes. *Genome Res.*, **13**, 1863–1872.
39. Ramaswamy,G., Karim,M.A., Murti,K.G. and Jackowski,S. (2004) PPARalpha controls the intracellular coenzyme A concentration via regulation of PANK1alpha gene expression. *J. Lipid Res.*, **45**, 17–31.
40. Trajkovski,M., Hausser,J., Soutschek,J., Bhat,B., Akin,A., Zavolan,M., Heim,M.H. and Stoffel,M. (2011) MicroRNAs 103 and 107 regulate insulin sensitivity. *Nature*, **474**, 649–653.
41. Chang,C.L., Au,L.C., Huang,S.W., Kwok,C.F., Ho,L.T. and Juan,C.C. (2010) Insulin up-regulates heme oxygenase-1 expression in 3T3-L1 adipocytes via PI3-kinase- and PKC-dependent pathways and heme oxygenase-1-associated microRNA downregulation. *Endocrinology*, **152**, 384–393.
42. Takada,I., Kouzmenko,A.P. and Kato,S. (2009) Molecular switching of osteoblastogenesis versus adipogenesis: implications for targeted therapies. *Expert Opin. Ther. Targets*, **13**, 593–603.
43. Zhang,Y., Xie,R.L., Croce,C.M., Stein,J.L., Lian,J.B., van Wijnen,A.J. and Stein,G.S. (2011) A program of microRNAs controls osteogenic lineage progression by targeting transcription factor Runx2. *Proc. Natl Acad. Sci. USA*, **108**, 9863–9868.
44. Gerin,I., Bommer,G.T., McCoin,C.S., Sousa,K.M., Krishnan,V. and MacDougald,O.A. (2010) Roles for miRNA-378/378* in adipocyte gene expression and lipogenesis. *Am. J. Physiol. Endocrinol. Metab.*, **299**, E198–E206.
45. Ortega,F.J., Moreno-Navarrete,J.M., Pardo,G., Sabater,M., Hummel,M., Ferrer,A., Rodriguez-Hermosa,J.I., Ruiz,B., Ricart,W., Peral,B. *et al.* (2011) MiRNA expression profile of human subcutaneous adipose and during adipocyte differentiation. *PLoS One*, **5**, e9022.